chemosensors

MDPI

Article

Multi-Element Prediction of Soil Nutrients Using Laser-Induced Breakdown Spectroscopy and Interpretable Multi-Output Weight Network

Xiaolong Li [1,†], Liuye Cao [1,†], Chengxu Lyu [2,*], Zhengyu Tao [3], Anan Tao [4], Wenwen Kong [3] and Fei Liu [1]

[1] National Key Laboratory of Agricultural Equipment Technology, College of Biosystems Engineering and Food Science, Zhejiang University, Hangzhou 310058, China; 11813010@zju.edu.cn (X.L.); 12313070@zju.edu.cn (L.C.); fliu@zju.edu.cn (F.L.)
[2] National Key Laboratory of Agricultural Equipment Technology, Chinese Academy of Agricultural Mechanization Sciences Group Co., Ltd., Beijing 100083, China
[3] College of Mathematics and Computer Science, Zhejiang A&F University, Hangzhou 311300, China; 2022611011056@stu.zafu.edu.cn (Z.T.); wwkong16@zafu.edu.cn (W.K.)
[4] Green Development Center, Bureau of Agriculture and Rural Affairs of Xiangshan County, Ningbo 315799, China; taoanan1984@163.com
* Correspondence: lvchengxu@caams.org.cn
† These authors contributed equally to this work.

Abstract

Rapid and green detection of soil nutrients is essential for soil fertility and plant growth. However, traditional methods cannot meet the needs of rapid detection, and the reagents easily cause environmental pollution. Hence, we proposed a multivariable output weighting-network (MW-Net) combined with laser-induced breakdown spectroscopy (LIBS) to achieve rapid and green detection for three soil nutrients. For a better spectral signal-to-background ratio (SBR), the two important parameters of delay time and gate width were optimized. Then, the spectral noise was removed by the near-zero standard deviation method. Three common quantitative models were investigated for single-element prediction, which are usually applied in LIBS analysis. Also, multi-element prediction was investigated using MW-Net. The results showed that MW-Net outperformed other models generally with very good quantification for soil total N and K (the determination coefficients in the prediction set (R_p^2) of 0.75 and 0.83 and the relative percent difference in the prediction sets (RPD) of 2.05 and 2.43) and excellent indirect determination for soil exchangeable Ca (R_p^2 of 0.93 and RPD of 3.91). Finally, the interpretability was realized through feature extraction from MW-Net, indicating its design rationality. The preliminary results indicated that MW-Net combined with LIBS technology could quantify the three soil nutrients simultaneously, improving the detection efficiency, and it could possibly be deployed on a LIBS portable instrument in the future for precision agriculture.

Keywords: soil; nutrients; LIBS; multi-element prediction; green detection

check for updates

Received: 29 July 2025
Revised: 25 August 2025
Accepted: 3 September 2025
Published: 5 September 2025

Citation: Li, X.; Cao, L.; Lyu, C.; Tao, Z.; Tao, A.; Kong, W.; Liu, F. Multi-Element Prediction of Soil Nutrients Using Laser-Induced Breakdown Spectroscopy and Interpretable Multi-Output Weight Network. *Chemosensors* **2025**, *13*, 336. https://doi.org/10.3390/chemosensors13090336

Copyright: © 2025 by the authors. Licensee MDPI, Basel, Switzerland. This article is an open access article distributed under the terms and conditions of the Creative Commons Attribution (CC BY) license (https://creativecommons.org/licenses/by/4.0/).

1. Introduction

Soil fertility is the basis for a healthy plant lifecycle, which has a great impact on crop quality and yield [1]. Soil fertility can be indicated by soil nutrients, including macro-nutrients, such as nitrogen (N), phosphorus (P), potassium (K), calcium (Ca), etc., and micro-nutrients, such as iron (Fe), manganese (Mn), etc. Among them, elements of N, P, and K were often added to commercial fertilizers, which are well known as NPK fertilizers [2].

N improves protein synthesis and leaf and vegetation growth [3]; P is beneficial for energy transfer and seeds and roots growth [3]; K serves water regulation and flower and grain growth [4]. Ca encourages the development of cytoderm, membrane, and enzymatic reactions [5]. Particularly, exchangeable Ca can influence the cation exchange capacity (CEC) greatly and affect plant uptake [6]. In this study, total N, K, and exchangeable Ca were the research targets.

When the soil nutrient contents are insufficient, they will be supplemented by fertilization to ensure the crop yield and quality. Inevitably, over- or underdosing may occur [7]. However, overdosing can cause surface exposure and water pollution. For example, the Baltic Sea is famous for "dead zones" because of excessive nutrient exposure of nitrogen (N) and phosphorus (P) [8]. And underdosing can lead to low levels of plant nutrients, thus reducing the crop quality and productivity. Precision agriculture (PA), defined by the International Society of Precision Agriculture, can solve this problem. To achieve PA, an accurate and fast detection method for soil nutrients is needed.

Traditional detection technologies include inductively coupled plasma-atomic emission spectrometry/mass spectrometry (ICP-AES/MS) [9], flame atomic absorption spectrometry (FAAS) [10], and so on. These methods are complex, time-consuming, and require an operator with a high level of expertise [11]. In addition, they often need a combination of chemical digestion to convert solid soil into a solution for instrument testing, easily causing secondary pollution [12].

Laser-induced breakdown spectroscopy (LIBS) has the advantages of rapid, non-contact, micro-destructive, multi-element, and small-sample detection [13], making it a good alternative for fast and green detection in agricultural fields [14]. In addition, the development of portable LIBS has made on-site detection a great possibility [15]. Quantitative detection of total N in fertilizer could be achieved by LIBS with a good linearity in the range from 1.72% to 5.98% [16]. Total K detection could also be realized by LIBS with the root mean square error of validation (RMSEV) of 0.0785 [17]. Except the total mass fractions of the elements, the mass fractions of available or soluble elements could also be successfully detected by LIBS. Soni et al. [12] used the P spectral line of 213.6 nm to detect the soluble P in soil with a detection limit of 0.27 mg/kg. Erler et al. [18] used the full spectra by portable LIBS combined with multivariate regression models to detect the total and available P for plants. Similarly, recent studies have shown that full-spectrum LIBS combined with multivariate models can also predict soil exchangeable cations. Pelagio et al. [19] demonstrated reliable prediction of soil cation exchange capacity (R^2 = 0.75, RPD = 2.0), while a more recent study [20] reported robust prediction of exchangeable Ca ($R^2 \approx 0.85$, RPD > 2.0) when calibrated against ammonium acetate extraction. These results indicate that exchangeable fractions, although not directly emitted, leave detectable spectral signatures associated with soil components, such as clay minerals and organic matter, and can therefore be inferred using LIBS with multivariate calibration. He et al. [21] applied multivariate regression models to realize the accurate detection of soil macro-nutrients (K, Ca, and Mg) and micro-nutrients (Fe, Mn, and Na). But these elements matched different optimal models. Erler also employed different models to detect multiple soil elements (Ca, K, Mg, N, P, Fe, Mn, and Al). At present, few scholars have tried to use a single model in LIBS technology to realize the accurate detection of multiple elements at the same time, which is helpful for the model deployment in a portable LIBS instrument.

Although LIBS fundamentally measures the total elemental emission from ablated soils, recent studies have shown that full-spectrum LIBS data combined with multivariate models can also capture information related to exchangeable cations.

In this study, we evaluated the potential of LIBS technology for the rapid and green detection of soil nutrients of total N, K, and exchangeable Ca. On the other hand, we tried

to design a multi-output model combined with the spectral wide band advantage of LIBS to achieve multiple elements detection simultaneously.

2. Materials and Methods

2.1. Soil Sample Preparation

In this study, the soil samples were collected from Jiangxi and Zhejiang provinces in paddy fields, including 50 and 152 samples, respectively. The sampling depth was the plough layer. The collected soil was air-dried first. Then, the samples were crushed, and impurities such as leaf residues and stones were removed. Finally, they were sifted through a 0.15 mm sieve to obtain powdery soil for later use.

Some soil powder samples were used for reference value measurement of total N, K, and exchangeable Ca. The measurement method adopted the corresponding Chinese standard methods (HJ 717-2014, NY/T 87-1988, NY/T 1121.13-2006) [22–24]. Table 1 shows the statistical results of the minimum, maximum, mean, and standard deviation values of total N, K, and exchangeable Ca content in the collected soil samples. For LIBS modeling, the model outputs were calibrated to chemical reference values, namely total N, total K, and exchangeable Ca.

Table 1. The statistical results of total N, K, and exchangeable Ca content in the soil samples.

Nutrient	Min	Max	Mean	S.D.
N (%)	0.01	0.24	0.10	0.05
K (g/kg)	13.70	49.94	25.45	6.31
Ca (mg/kg)	98.12	12,064.97	3880.04	3607.35

The other samples were used for the sample preparation of LIBS experiment. For ensuring reproducible laser–sample interaction and the measurement precision, the soil samples were usually processed into homogeneous tablets [25]. In this study, 0.5 g soil powders were weighed into a circular die, and then the circular die was shaken to ensure smooth top surface of soil powder and then pressed at 20 MPa for 30 s using a tablet machine. Uniform soil tablets with a diameter of about 15 mm were produced. Notably, the samples for LIBS experiment were prepared without any chemical treatment.

2.2. LIBS Setup

Figure 1 shows the self-assembled LIBS system. The optical reflection system guided the laser to soil tablets, in which slide and polarizer were combined to adjust the laser energy, and lens was used to focus the laser. The laser was from Q-switched Nd:YAG pulse laser (Vlite-200, Beamtech Optronics, Beijing, China) with 532 nm and a pulse duration of 8 ns. The spectrometer (ME5000, Andor, Belfast, UK) was applied to disperse light at a range of about 200–900 nm, and then the light was converted into electrical signals by ICCD (DH334, Andor Information Technology Ltd., Belfast, UK) and recorded on the computer. The delay generator was used to improve the signal quality by controlling the specific spectrum acquisition time after laser emission. When the laser energy was greater than 70 mJ, the laser would stir up serious soil dust, which could be easily adsorbed onto the lens, hindering the laser propagation. Thus, the laser energy was optimized to 70 mJ.

To minimize laser-induced point-to-point fluctuations, the laser ablation path was configured 4 × 4 array of 16 different positions with five consecutive ablations at each position. Therefore, a total of 80 spectra were collected on a soil tablet. Because the laser frequency was 1 Hz, it took only 80 s to complete the spectral acquisition. Thus, it was a fast scheme.

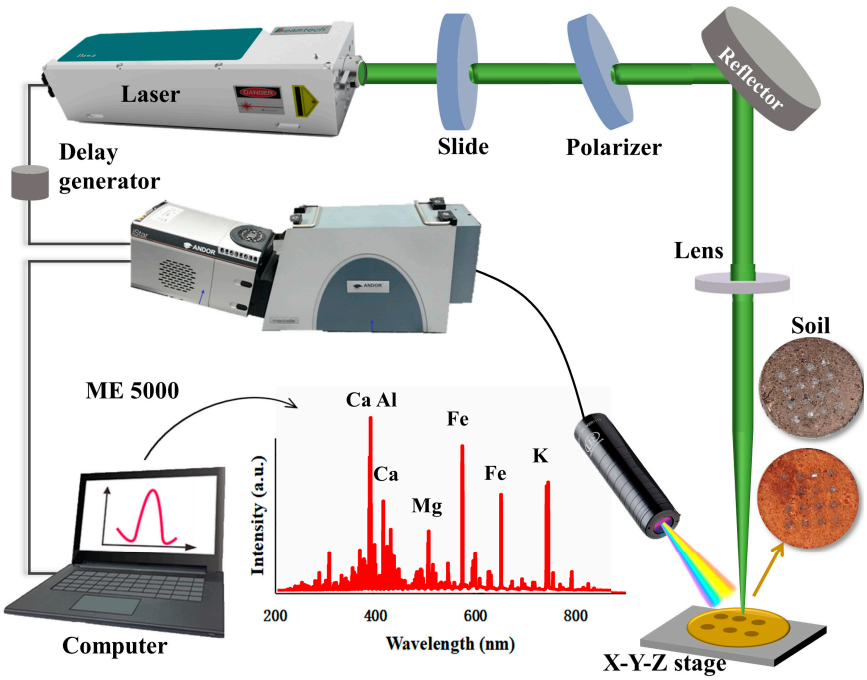


Figure 1. The scheme of the LIBS experiment.

2.3. Qualitative and Quantitative Models

2.3.1. PCA Analysis

Principal component analysis (PCA) is an unsupervised and multivariate qualitative analysis method that is often used in LIBS analysis [26]. The principle of PCA is to project the original spectral variables onto different direction vectors to reduce the spectral dimension and retain the valid information [27]. The data after projection through different direction vectors is called principal components (PCs). And each PC corresponds to an explained variance and PCA loading, which reflect the retention degree of the original information and the spectral variable importance, respectively [28]. In this study, by plotting the 3D scatter of the first three PCs, the clustering effect of soil samples from different places could be intuitively observed. By plotting PCA loadings, important variables could be recognized.

2.3.2. Machine Learning

Partial least squares regression (PLSR) is typical multivariate method of machine learning for LIBS analysis [29]. For spectral analysis, PLSR could mine the linear relationship between spectral variables and the concentration of the target element [30], so, in addition to quantitative analysis, it could also be used as a feature extraction analysis. The regression coefficients of PLSR could be used to extract feature spectral variables of LIBS [31]. PLSR could mine linear relationships, while least squares support vector machine (LS-SVM) and extreme learning machine (ELM) could mine non-linear relationships for LIBS analysis. LS-SVM was a variant of SVM, the principle of which was to distinguish samples of different concentrations or species through hyperplanes while minimizing structural risk [32]. And the determination of hyperplanes could mine non-linear relationships. ELM is a single hidden layer feedforward neural network (SLFNN), in which the weights between the input and hidden layers are randomly assigned and kept fixed, while the output weights are determined analytically using a least-squares solution [33]. The rectified linear unit (Relu) activation function in SLFNN could mine non-linear relationship. In this study, machine learning methods of PLSR, LS-SVM, and ELM were applied for soil nutrients LIBS detection, in which LS-SVM and ELM were used for single-element prediction and PLSR for

both single- and multi-element prediction. The optimized parameters of the single-element prediction models are summarized in Table 2. For the multi-element prediction, the PLSR model was optimized with the number of latent variables set to 10. They were built on Matlab R2020b (The MathWorks, Natick, MA, USA).

Table 2. Optimized parameters of PLSR, ELM, and LS-SVM models for single-element prediction of soil nutrients (N, K, and exchangeable Ca).

Nutrient	PLSR	ELM	LS-SVM	
	LVs	H	γ	C
N	14	643	59,856.97	1,270,255.64
K	15	931	50,949.45	274,524.95
Ca	10	857	44,081.72	56.98

Note: LVs: latent variables. H: Number of Hidden Neurons. γ: Kernel Function Parameter. C: Error Penalty Factor.

2.3.3. MW-Net Design

In order to realize a model to predict multi-elements of soil nutrients simultaneously, we designed a multivariable output weighting-network (MW-Net). Figure 2 shows its framework. MW-Net had four layers in total. The first layer was the soil LIBS spectrum input layer, which was used to accept the input. After removing noise, the soil spectrum had 16,864 spectral variables. Because the neurons should correspond to the spectral variables one by one, 16,864 neurons were set in this layer. The second layer was the weight-transformed layer, which was used to initially assign higher weights to important spectral variables. The input of this layer was the neuron value from the first layer. The output of this layer was obtained by multiplying the input by the weight coefficient (α), in which α was updated by network self-learning mechanism of SGD algorithm. In addition, a trainable bias term was included in this layer, and the output was passed through a rectified linear unit (ReLU) activation function to capture non-linear relationships and enhance model stability. Therefore, the output also had 16,864 neurons in this layer. The third layer was the parallel fully connected layer, which was used to preliminarily predict the contents of N, K, and Ca in five parallel. The input data was the neuron value from the second layer. The output of this layer was obtained by transforming the input data into five groups of neurons through the fully connected mechanism, in which every group had three neurons representing the initial predicted content of N, K, and Ca, respectively. Each branch included both weight and bias parameters and applied ReLU activation after the linear transformation. Thus, the output had 15 neurons in this layer. The fourth layer was the weighted multivariable output layer, which was used to output the final predicted content of N, K, and Ca simultaneously. The input data was the values of 15 neurons of the third layer. Taking N as an example, the output of this layer was obtained by multiplying the initial five parallel contents of N with five weights (W_N) and then summed to the final content of N, in which the value of W_N was obtained in the same way as α. The final contents of K and Ca were also obtained using the same method in parallel. Unlike the previous layers, no activation function was applied here, so the network produced linear outputs suitable for regression. The final regression layer consisted of three neurons corresponding to total N, total K, and exchangeable Ca. Therefore, the output had three neurons in the last layer. By assigning different weights to all wavelengths in the input layer, MW-Net can automatically emphasize spectral variables correlated with target elements and suppress those dominated by background variability, thereby reducing matrix sensitivity.

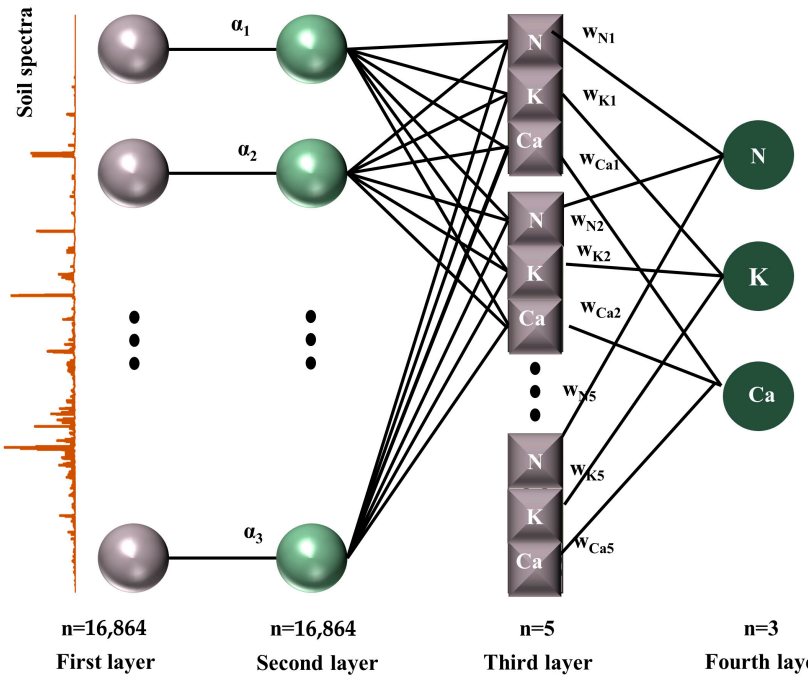


Figure 2. The framework of MW-Net.

2.4. Model Evaluation Indexes

The determination coefficient (R^2) could assess the interpretation degree of spectral intensity to element concentration, which was between 0 and 1. The closer to 1, the better the effect [33]. The root mean square error (RMSE) could evaluate the deviation between the reference value of Cd concentration and the predicted values by models, which could directly reflect the model prediction effect. The ratio of standard deviation of the prediction to RMSEP (RPD) could assess the model stability. A good model was obtained with an R^2 close to 1, small RMSE, and large RPD. For RPD in soil science, the value was less than 1 with a poor model quantification; between 1.4 and 1.8 with a fair model for assessment and correlation; between 1.8 and 2.0 with a possible model quantification; between 2.0 and 2.5 with a very good model quantification; and more than 2.5 with an excellent quantification [34,35]. RMSE in validation and prediction sets were labeled as RMSEV and RMSEP.

The formulas were as follows: n represented the number of soil tablets, y represented the concentration reference value of the object element, and $\overline{y}$ represented the corresponding average value of y. $\hat{y}_i$ represented the concentration predicted value of the object element.

$$R^2 = 1 - \frac{\sum_{i=1}^{n}(\hat{y}_i - y_i)^2}{\sum_{i=1}^{n}(y_i - \overline{y})^2} \quad (1)$$

$$\mathrm{RMSE} = \sqrt{\frac{\sum_{i=1}^{n}(\hat{y}_i - y_i)^2}{n}} \quad (2)$$

$$\mathrm{RPD} = \sqrt{\frac{\sum_{i=1}^{n}(y_i - \overline{y})^2}{n}} / RMSEP \quad (3)$$

3. Results and Discussion

3.1. LIBS Parameter Optimization

Delay time and gate width were the two important parameters that affected the SBR of the LIBS spectra. In order to capture enough spectral signal before the plasma disappeared,

the sum of the delay time and gate width was set to 20 μs. In this study, the delay time was set as 0.5, 1, 1.5, 2, 2.5, 3, 3.5, 4, 4.5, 5, 5.5, and 6 μs, respectively. When the delay time was as low as 0.5 or 1 μs, the LIBS spectra had pronounced background noise (as shown in Figure S1). Therefore, the delay time after 1 μs was analyzed. Figure 3 shows the SBR of N, K, and Ca spectral lines with different delay times after 1 μs. The corresponding error bar was produced from 16 spectra in one soil tablet. Element fingerprint lines in LIBS could be queried through the National Institute of Standards and Technology (NIST) [36]. For the N spectral line of 383.44 nm, the SBR rose sharply before 2.5 μs, then slowly rose and levelled off after 4 μs. For the two K spectral lines of 766.54 and 769.94 nm, both SBRs rose first and then became stable, and a stable SBR was observed after 2.5 μs. For the two Ca spectral lines of 393.36 and 396.85 nm, both SBRs rose first and then fell, with the highest point at 2 μs. Therefore, for overall consideration of the three elements, the delay time could be set as 2.5 μs, and good SBRs could be obtained for them. Then, the corresponding gate width was 17.5 μs.

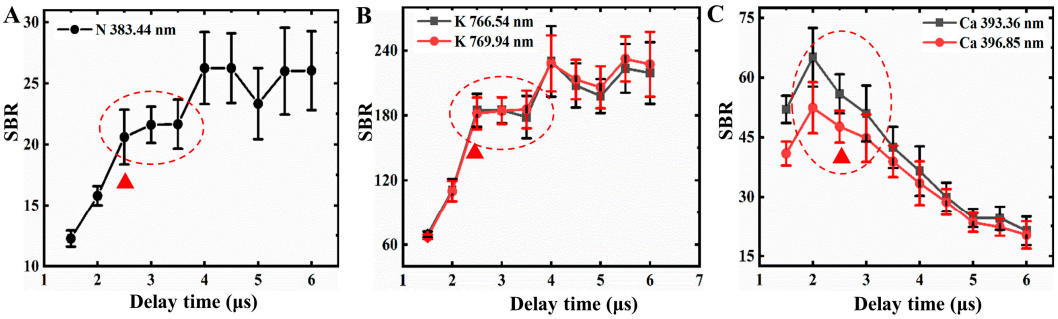


Figure 3. The SBR of (**A**) N, (**B**) K, and (**C**) Ca spectral lines with different delay times. Note: The red dotted circles indicate the key delay-time regions where SBR changes significantly, and the red triangle marks the selected optimal delay time (2.5 μs).

3.2. Average Spectra Analysis

LIBS technology had the advantage of multi-element analysis because the LIBS spectrum had a large wavelength range, which could indicate a variety of elements. Figure 4 shows the soil average LIBS spectra of the 202 soil samples under the above optimal LIBS parameters.

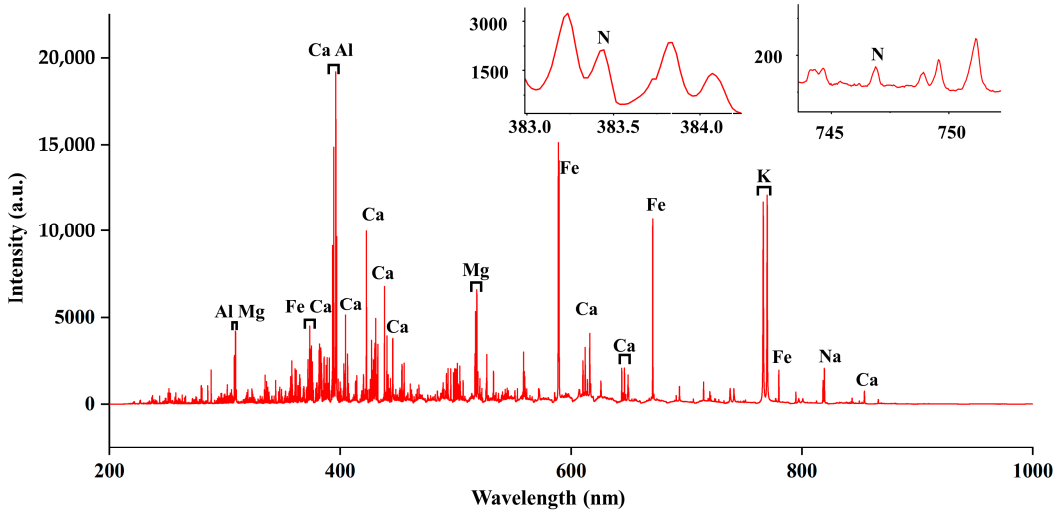


Figure 4. The soil average LIBS spectra under the optimal LIBS parameters.

It was found that a broad range of soil typical nutrient elements were emitted, including major elements such as N (383.44, 746.92 nm, etc.), K (766.54, 769.94 nm, etc.), medium elements such as Ca (393.36, 396.85, 612.30 nm, etc.) and Mg (516.76, 517.30, 518.37 nm, etc.), minor elements such as Fe (588.98, 589.60, 670.81 nm, etc.), and so on. There were also many other unlabeled emitted lines in the LIBS spectrum in the large range of 200–900 nm. However, a large wavelength range could also contain a large number of useless spectral lines and background noise, which would interfere with the target elements detection. Therefore, spectral denoising was needed to reduce the interference of useless spectral variables.

3.3. Spectra Noise Elimination

Noise wavelengths caused information redundancy and reduced prediction accuracy, which should be removed. The intensities of noise wavelengths varied slightly in all soil samples, while those of information wavelengths varied largely, reflecting soil characteristics. Relying on the difference, wavelengths with low standard deviation intensity could be considered as noise wavelengths to some extent. Figure S2 shows the standard deviations for all wavelengths arranged in order from smallest to largest. It was observed that there were about 10,000 wavelengths with standard deviations near 0, indicating that these wavelengths did not vary much in the soil samples. Thus, these 10,000 wavelengths were eliminated.

Figure 5 shows the original spectra and noise wavelengths-eliminated spectra. We could find that the number of wavelengths in a soil LIBS spectrum was reduced from 26,864 to 16,864, removing more than 1/3 of the spectral wavelengths. But the overall spectral profile was almost unchanged, and the information wavelengths with higher intensity were retained. This indicated that spectral noise was effectively removed, and useful spectral information was effectively retained. The denoised spectra were used for the next analysis of soil nutrients.

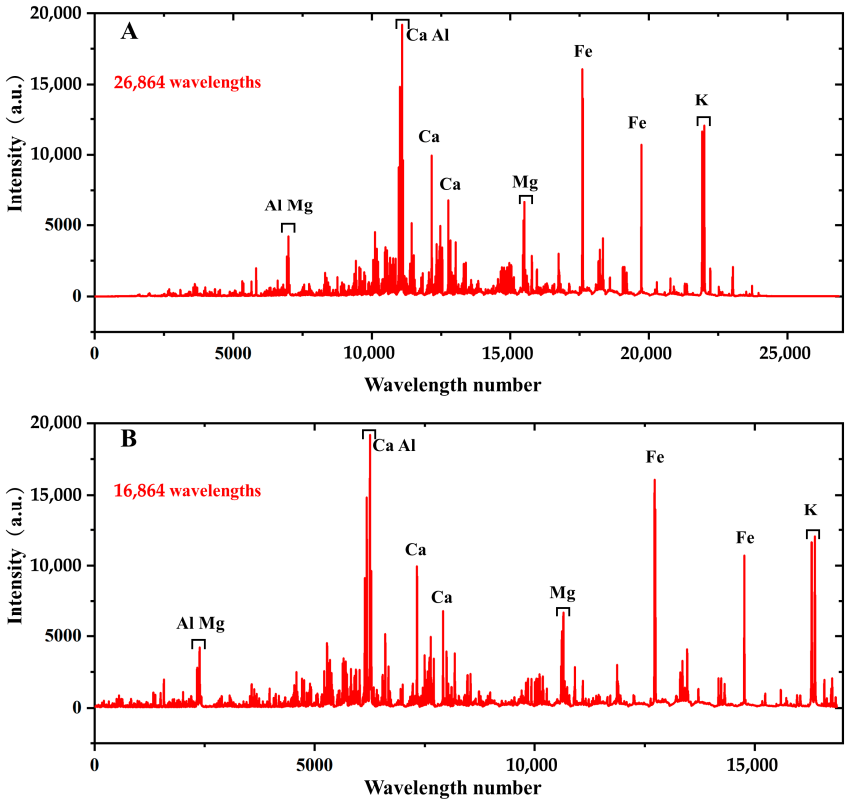


Figure 5. Comparison of soil LIBS spectra: (**A**) original spectra and (**B**) noise wavelengths-eliminated spectra.

3.4. Qualitative Analysis

The clustering effect of soil samples from different provinces was investigated by PCA analysis. There were 152 and 50 samples from Zhejiang and Jiangxi provinces. Figure 6A shows the 3D scatter plot of soil samples based on the first three PCs. It was observed that the first three PCs explained 97.2% of the variation with a PC1 of 77.3, PC2 of 15.3, and PC3 of 4.6%. Soils from the two different provinces were clearly grouped into two clusters, which indicated that the spectral differences of soils could be successfully recognized by PCA. Figure 6B shows the important variables by PCA loadings. Loading in PC1 with the largest explained variance recognized more important variables than those in PC2 and PC3. The common important variables for all three PCs were Ca, Al, Fe, and K. Perhaps, the content and proportion of these elements played a very important role in soil clustering.

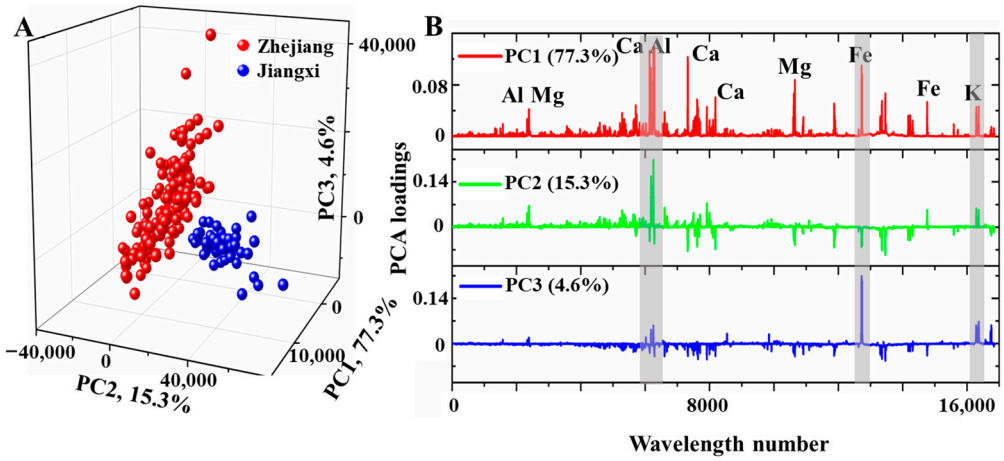


Figure 6. (**A**) Three-dimensional scatter plot of soil samples from Zhejiang and Jiangxi provinces based on the first three PCs and (**B**) the important variables by PCA loadings. Note: The gray area highlight the spectral ranges that contribute significantly to soil clustering.

3.5. Quantitative Analysis

3.5.1. Data Splitting and Preprocessing

The 202 soil samples were randomly split into a calibration set, validation set, and prediction set at a ratio of approximately 3:1:1. It was worth noting that the samples corresponding to the minimum and maximum values of the three elements must be put into the calibration set for model training. Among them, the calibration set and validation set were used to build the model, and the prediction set was used to test the model. The number of soil samples in the corresponding sets was 124, 39, and 39, respectively. The corresponding LIBS spectra numbers were also 124, 39, and 39, respectively.

For spectral data, area normalization was used to minimize the laser fluctuation error from point to point [37]. For nutrient reference value data, z-score normalization was applied to convert three different ranges of nutrient element values into the same level space for multi-element prediction. Notably, the means and variances required for the z-score were generated from the calibration set and then used in the validation and prediction set to ensure the quantification rationality.

3.5.2. Single-Element Prediction

Researchers usually optimized models of quantifying a single element rather than multiple elements [29]. Because single-element prediction tended to yield better results than multi-element prediction using the same model. In this study, three common LIBS quantitative models, namely PLSR, ELM, and LS-SVM, were built and compared in single-element prediction. Table 3 shows the results. For both N and K prediction, the optimal

model was PLSR, with an R^2_P value of 0.68 and 0.87, RMSEP value of 2% and 1.99 g/kg, and RPD value of 2.05 and 2.85, respectively. For the Ca indirect determination, the optimal model was ELM, with an R^2_P value of 0.92, RMSEP value of 950.99 mg/kg, and RPD value of 3.60. The next best model was PLSR with the same R^2_P and a slightly higher RMSEP and RPD. Overall, PLSR was a suitable model for retrieving soil nutrient elements using LIBS spectra. The RPD value of N was more than 2, indicating a very good prediction, and those of K and Ca were both more than 2.5, indicating an excellent prediction.

Table 3. The results of single-element prediction of N, K, and exchangeable Ca based on three models.

Model	Single Nutrient	R^2_V	RMSEV	R^2_P	RMSEP	RPD
PLSR	N	0.41	0.03	0.68	0.02	2.05
	K	0.75	2.91	0.87	1.99	2.85
	Ca	0.93	951.40	0.92	951.53	3.59
ELM	N	0.34	0.03	0.65	0.02	2.05
	K	0.81	2.56	0.85	2.17	2.61
	Ca	0.95	815.67	0.92	950.99	3.60
LS-SVM	N	0.34	0.03	0.66	0.02	2.05
	K	0.76	2.86	0.78	2.63	2.15
	Ca	0.94	874.54	0.91	987.69	3.46

Note: N, K, and Ca represented total N, total K, and exchangeable Ca in soil. Their corresponding units of RMSE were %, g/kg, and mg/kg, respectively.

However, different quantitative models or different parameters of the same model increased the algorithm complexity, which was not conducive to the model deployment in LIBS portable instruments. Therefore, it was also necessary to investigate one model to accurately quantify the three soil nutrients simultaneously.

3.5.3. Multi-Element Prediction

A single LIBS spectrum contained large soil element information, so it had the potential to use one model to achieve multi-element prediction. From the above results, PLSR obtained the better performance in single-element prediction of N, K, and Ca, and PLSR itself could also serve as a multi-element prediction model. Therefore, PLSR was selected as a comparation with MW-Net for multi-element prediction. Table 4 shows the comparation results. MW-Net performed better than PLSR for all three nutrients of N, K, and Ca. The corresponding optimal R^2_P values were 0.75, 0.83, and 0.93; the RMSEP values were 2%, 2.33 g/kg, and 873.78 mg/kg; and the RPD values were 2.05, 2.43, and 3.91, respectively. Notably, the quantitative effects of N and Ca were even better than those for the optimal results of single-element prediction by PLSR, indicating the rationality and effectiveness of the designed MW-Net. The RPD values for N and K were more than 2, and for Ca, it was more than 2.5, indicating that MW-Net combined with LIBS technology could simultaneously achieve very good prediction for soil total N and K and excellent indirect determination for soil exchangeable Ca. The performance of MW-Net across more than 200 diverse soil samples suggests a reduced sensitivity to matrix effects. For instance, the prediction R^2_P increased from 0.43 to 0.75 for N and from 0.72 to 0.83 for K compared with PLSR, indicating that MW-Net could extract more stable spectral features despite variations in soil composition.

Table 4. The results of multi-element prediction of N, K, and exchangeable Ca based on PLSR and MW-Net.

Model	Multi Nutrients	R^2_V	RMSEV	R^2_P	RMSEP	RPD
PLSR	N	0.15	0.04	0.43	0.03	1.37
	K	0.62	3.59	0.72	2.97	1.91
	Ca	0.93	951.38	0.92	951.55	3.59
MW-Net	N	0.46	0.03	0.75	0.02	2.05
	K	0.77	2.79	0.83	2.33	2.43
	Ca	0.93	917.37	0.93	873.78	3.91

Note: N, K, and Ca represented total N, total K, and exchangeable Ca in soil. Their corresponding units of RMSE were %, g/kg, and mg/kg, respectively.

Figure 7 visually shows the scatter plots of multi-element prediction based on MW-Net in the prediction set of N, K, and Ca, respectively. The blue, red, and green dashed lines were the corresponding linear fitting lines between the reference and prediction values, of which the formulas and R^2 were marked. For N, K, and Ca, the R^2 values were 0.75, 0.83, and 0.94, respectively. The prediction effects became better and better. The reason might be that a high transition probability of the element line could increase the LIBS quantitative ability [38]. The transition probability was generally ordered as Ca > K > N in NIST. On the whole, the scatter points of all the elements were close to the y = x line, indicating that MW-Net combined with LIBS technology could quantify the three soil nutrients simultaneously.

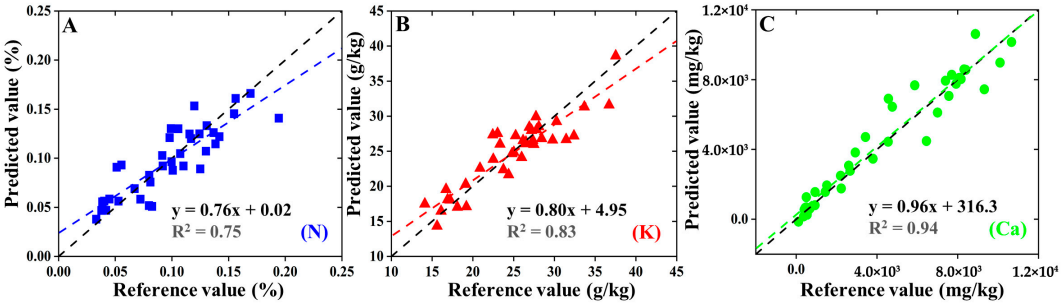


Figure 7. The scatter plots of multi-element prediction in the prediction set for (**A**) N, (**B**) K, and (**C**) Ca based on MW-Net. Note: Blue squares, red triangles, and green circles represent the prediction results for N, K, and Ca, respectively. The black dotted line indicates the 1:1 reference line, while the colored dotted line show the regression fits for each element.

3.6. Comparison and Discussion

3.6.1. Comparison of MW-Net and PLSR

MW-Net of multi-element prediction and PLSR of single-element prediction obtained better performance in N, K, and Ca prediction. The important spectral wavelength concerned by the two models was compared. For PLSR, the regression coefficient could indicate the important spectral wavelength [31]. For MW-Net, the transformed spectra from the third layer had the same effects. Regression coefficient and transformed spectra were collectively called the weight coefficient for ease of description. The greater the weight coefficient, the more important the corresponding wavelength. Figure 8 shows the comparative results, in which A meant the model and B meant the object nutrient. For example, A-B of PLSR-N meant that the weight coefficient was from the PLSR model of single-element prediction for total N determination. C (D) of MW-Net (N) meant that the weight coefficient was from the MW-Net model of multi-element prediction for total N determination.

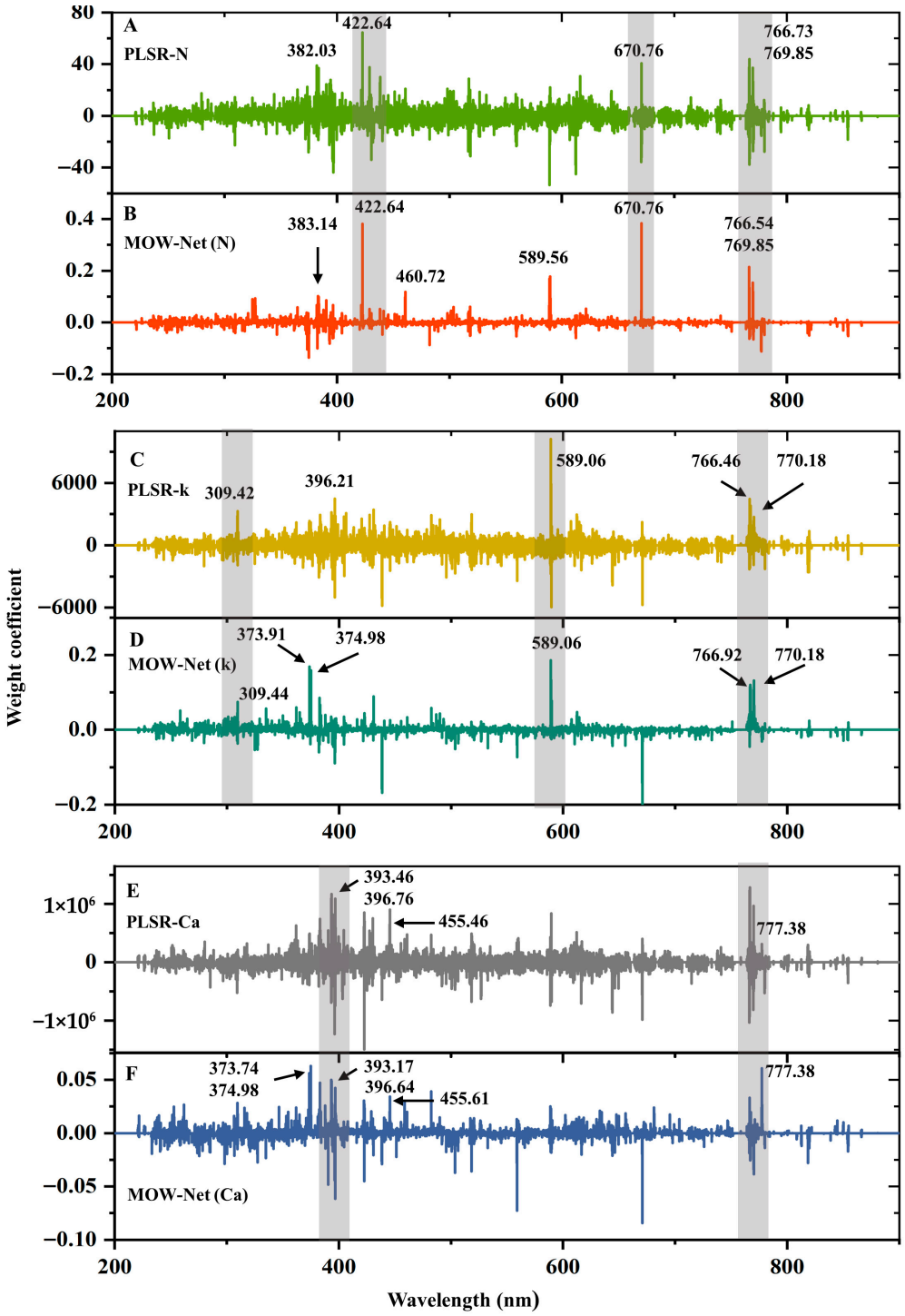


Figure 8. A-B meant that the weight coefficient was extracted from A model for B determination. (**A**) PLSR-N, (**B**) MW-Net-N, (**C**) PLSR-K, (**D**) MW-Net-K, (**E**) PLSR-Ca, and (**F**) MW-Net-Ca. Note: The grey area highlight the important wavelength ranges, and the arrows indicate the corresponding characteristic spectral lines.

Overall, PLSR and MW-Net focused on similar wavelengths for all three target nutrients. However, the line shape from PLSR had a wider band around the 0 baseline, while that from MW-Net had a smaller one, which indicated that the MW-Net model could concentrate more on the important wavelength with less interference from other wavelengths. This might be one of the reasons why MW-Net achieved better prediction results than PLSR.

For N prediction, from Figure 8A based on PLSR, the important wavelengths were 382.03, 422.64, 670.76, 766.73, and 769.85 nm. The similar and corresponding wavelengths based on MW-Net (Figure 8B) were 383.14, 422.64, 670.76, 766.54, and 769.85 nm. The N fingerprint wavelengths queried from NIST were (381.82, 382.20, 383.04, 383.42), 422.77, and (670.61, 670.87) nm. Therefore, their important wavelengths had a certain correlation with the N fingerprint wavelengths. However, the wavelengths about 766 and 769 nm had a correlation with K instead of N. The reason might be that the K element could influence the N prediction. Notably, MW-Net concerned two more spectral lines than PLSR of 460.72 and 589.56 nm. The corresponding N fingerprint wavelengths could also be queried in NIST with 460.72 and 589.72 nm. This might be one of the reasons why MW-Net achieved better N prediction.

For K prediction, from Figure 8C based on PLSR, the important wavelengths were 309.42, 589.06, 766.46, and 770.18 nm. The similar wavelengths from MW-Net (Figure 8D) were 309.44, 589.06, 766.92, and 770.18 nm. The K fingerprint wavelengths queried from NIST were (310.18, 310.2) and (766.48, 769.90) nm. Therefore, their concerned wavelengths had a certain correlation with the K fingerprint wavelengths. The 589.06 nm wavelength had a correlation with Fe, which might influence the K prediction. In addition, PLSR concerned a different wavelength of 396.21 nm, while MW-Net concerned two different wavelengths of 373.91 and 374.98 nm. All their corresponding K fingerprint wavelengths could be queried in 396.67 and (373.91, 374.44) nm. But 396.67 nm had a higher transition probability. This might be the reason why PLSR achieved a slightly better K prediction than MW-Net.

For Ca prediction, from Figure 8E, based on PLSR, the important wavelengths were 393.46, 396.76, 455.46, and 777.38 nm. The similar wavelengths from MW-Net (Figure 8F) were 393.17, 396.64, 455.61, and 777.38 nm. Some corresponding wavelengths were slightly offset. The Ca fingerprint wavelengths queried from NIST were 393.36, 396.84, 455.46, and 777.71 nm. Therefore, their concerned wavelengths had a certain correlation with the Ca fingerprint wavelengths. Notably, MW-Net concerned two more spectral lines than PLSR in 373.74 and 374.98 nm. The corresponding Ca fingerprint wavelengths could also be queried in NIST of (373.69, 373.93) and (374.84, 375.02) nm. This might cause better Ca indirect determination for MW-Net than PLSR.

3.6.2. Multi-Output Model Exploration

Although some machine learning (ML) models can also be used as multi-output regression, such as random forest regressor (RFR) [39], k-nearest neighbor (KNN) [40], and extreme learning machine (ELM) [41], etc., these models for multi-output prediction find it difficult to achieve better results than single-output prediction. Therefore, most researchers used single-output ML models for LIBS classification or prediction [42]. In this study, similar results were found in that single-output PLSR (Table 3) outperformed multi-output PLSR (Table 4) in N, K, and Ca prediction. The reason might be that ML has its own inherent data learning mode, and the learning results are different for different objects, so it is difficult to strike a balance. For example, in this study, PLSR mainly relying on linear learning mode had learned different important wavelengths for the three elements (Figure 8), so it is hard to strike a balance in the PLSR linear calculation considering the three elements simultaneously. Fortunately, the data-driven neural network algorithm with SGD optimization is appropriate for multi-output prediction because of its flexible learning mechanism and calculation architecture. A neural network-based model had been designed as a multi-output regression model for estimating all key hypotheses in a single training process [43]. A convolutional neural network (CNN)-based model had also been designed as a multi-output model for monitoring multiple state properties in laser welding [44].

However, the application of multi-output regression to soil analysis using LIBS was still rare. In this study, the neural network-based MW-Net was proven to be able to achieve accurate multi-element prediction for soil nutrients by LIBS. And the spectral interpretation was realized, showing that the multi-output model could focus on the similar important wavelengths with the optimal single-output model of PLSR, indicating its rationality. MW-Net could provide some insights into the multi-output model design for multi-element prediction using LIBS. In addition, it will be a good exploration of the predicted elements that are related to each other. In the future, other flexible learning mechanisms such as convolution [45] and residual [46] can be investigated for LIBS multi-output regression.

3.6.3. Limitations and Future Perspectives

While the proposed MW-Net combined with LIBS demonstrated promising results for multi-element prediction, some limitations should be acknowledged and may guide future improvements. It should be noted that the LIBS measurements of nitrogen in this study were conducted in ambient air without the use of an argon jet. This choice was intentional, as our primary objective was to evaluate the feasibility of a simple and portable configuration for simultaneous multi-element analysis (N, K, and exchangeable Ca), which is more consistent with the practical requirements of in situ soil nutrient monitoring. While interference from atmospheric nitrogen emissions may affect sensitivity, our results demonstrate that acceptable prediction accuracy (Rp^2 = 0.75, RPD = 2.05) can still be achieved under these conditions. Previous studies [16,18] have shown that argon-assisted LIBS can further enhance the signal-to-noise ratio for nitrogen detection, and future work will consider integrating this strategy to improve the accuracy and robustness of N analysis while maintaining the practicality of multi-element, in-field measurements. In addition, although P is a vital soil nutrient, it was not investigated in this study due to the weak ultraviolet emission lines of P and its generally low concentrations in soil, particularly for plant-available P. These factors constrain the sensitivity and accuracy of conventional LIBS-based quantification. Future research should therefore focus on advanced LIBS approaches, such as laser-induced fluorescence-assisted LIBS, to enhance the detection and quantification of phosphorus. Incorporating such techniques would extend the applicability of the model and facilitate more reliable in-field assessment of phosphorus, which is critical for precision agriculture.

Matrix effects and self-absorption are well-known challenges in LIBS analysis. In this study, MW-Net alleviated matrix effects by assigning different weights to all input wavelengths and suppressing variability not related to nutrient concentrations. Similarly, since the model learns from multiple spectral variables simultaneously, it is less dependent on single emission lines such as K I, which may suffer from self-absorption. Nevertheless, these issues cannot be completely avoided and will require continued attention in future work.

4. Conclusions

This paper provided an interpretable and multi-element prediction model (MW-Net) for LIBS prediction in soil total N, K, and exchangeable Ca. In the prediction set, the corresponding R^2 values were 0.75, 0.83, and 0.93; the RMSEP values were 2%, 2.33 g/kg, and 873.78 mg/kg; and the RPD values were 2.05, 2.43, and 3.91, respectively. The results indicated that MW-Net combined with LIBS technology could achieve very good prediction for soil total N and K and excellent indirect determination for soil exchangeable Ca, simultaneously. Notably, the results were even better than those of PLSR under single-element quantification, indicating the superior performance of our designed MW-Net. This paper

also provided a rapid, effective, and green soil detection scheme, which was of certain reference value for precision agriculture.

Supplementary Materials: The following supporting information can be downloaded at: https://www.mdpi.com/article/10.3390/chemosensors13090336/s1, Figure S1: Soil spectra under the delay time of 0.5 and 1 μs; Figure S2: The standard deviations arranged in order from smallest to largest for all wavelengths.

Author Contributions: Conceptualization, X.L., Z.T., A.T., and F.L.; methodology, X.L., Z.T., W.K., and F.L.; software, X.L. and C.L.; validation, X.L.; formal analysis, X.L.; investigation, X.L.; resources, F.L.; data curation, L.C.; writing—original draft preparation, X.L.; writing—review and editing, L.C., C.L., Z.T., A.T., W.K., and F.L.; visualization, X.L.; supervision, F.L.; project administration, F.L.; funding acquisition, F.L. All authors have read and agreed to the published version of the manuscript.

Funding: This study was supported by the Opening Fund of National Key Laboratory of Agricultural Equipment Technology (NKL-2023-002), the National Natural Science Foundation of China (32371986), and the Ningbo Science and Technology Bureau (2024S099).

Institutional Review Board Statement: Not applicable.

Informed Consent Statement: Not applicable.

Data Availability Statement: The datasets presented in this article are not readily available because they contain proprietary information specific to our research project.

Conflicts of Interest: Author Lyu was employed by the company Mechanization Sciences Group Co., Ltd. The remaining authors declare that the research was conducted in the absence of any commercial or financial relationships that could be construed as a potential conflict of interest. The authors declare no conflicts of interest.

References

1. Albuquerque, J.R.D.P.; Makara, C.N.; Ferreira, V.G.; Brazaca, L.C.; Carrilho, E. Low-cost precision agriculture for sustainable farming using paper-based analytical devices. *RSC Adv.* **2024**, *14*, 23392–23403. [CrossRef] [PubMed]
2. Ji, L.; Xu, X.; Zhang, F.; Si, H.; Li, L.; Mao, G. The Preliminary Research on Shifts in Maize Rhizosphere Soil Microbial Communities and Symbiotic Networks under Different Fertilizer Sources. *Agronomy* **2023**, *13*, 2111. [CrossRef]
3. Potdar, R.P.; Shirolkar, M.M.; Verma, A.J.; More, P.S.; Kulkarni, A. Determination of soil nutrients (NPK) using optical methods: A mini review. *J. Plant Nutr.* **2021**, *44*, 1826–1839. [CrossRef]
4. Cakmak, I.; Rengel, Z. Humboldt Review: Potassium may mitigate drought stress by increasing stem carbohydrates and their mobilization into grains. *J. Plant Physiol.* **2024**, *303*, 154325. [CrossRef]
5. Ameer, S.; Ibrahim, H.; Kulsoom, F.N.U.; Ameer, G.; Sher, M. Real-time detection and measurements of nitrogen, phosphorous & potassium from soil samples: A comprehensive review. *J. Soils Sediments* **2024**, *24*, 2565–2583. [CrossRef]
6. Lv, H.; Pang, Z.; Chen, F.; Ji, H.; Wang, W.; Zhou, W.; Dong, J.; Li, J.; Liang, B. Effects of Cultivation Years on the Distribution of Nitrogen and Base Cations in 0–7 m Soil Profiles of Plastic-Greenhouse Pepper. *Agronomy* **2024**, *14*, 1060. [CrossRef]
7. Zhang, J.; Wang, R.; Jin, Z.; Guo, H.; Liu, Y.; Chang, Y.; Chen, J.; Li, M.; Chen, X. Development of On-Site Rapid Detection Device for Soil Macronutrients Based on Capillary Electrophoresis and Capacitively Coupled Contactless Conductivity Detection (C4D) Method. *Chemosensors* **2022**, *10*, 84. [CrossRef]
8. Andersen, J.H.; Carstensen, J.; Conley, D.J.; Dromph, K.; Fleming-Lehtinen, V.; Gustafsson, B.G.; Josefson, A.B.; Norkko, A.; Villnäs, A.; Murray, C. Long-term temporal and spatial trends in eutrophication status of the Baltic Sea. *Biol. Rev.* **2017**, *92*, 135–149. [CrossRef]
9. Moor, C.; Lymberopoulou, T.; Dietrich, V.J. Determination of Heavy Metals in Soils, Sediments and Geological Materials by ICP-AES and ICP-MS. *Microchim. Acta* **2001**, *136*, 123–128. [CrossRef]
10. Basiri, S.; Moinfar, S.; Hosseini, M.R.M. Determination of As(III) using developed dispersive liquid–liquid microextraction and flame atomic absorption spectrometry. *Int. J. Environ. Anal. Chem.* **2011**, *91*, 1453–1465. [CrossRef]
11. Wang, W.; Man, Z.; Li, X.; Zhao, Y.; Chen, R.; Pan, T.; Wang, L.; Dai, X.; Xiao, H.; Liu, F. Multi-phenotype response and cadmium detection of rice stem under toxic cadmium exposure. *Sci. Total Environ.* **2024**, *917*, 170585. [CrossRef]
12. Soni, S.; Viljanen, J.; Uusitalo, R.; Veis, P. Phosphorus quantification in soil using LIBS assisted by laser-induced fluorescence. *Heliyon* **2023**, *9*, e17523. [CrossRef]

13. Hahn, D.W.; Omenetto, N. Laser-induced breakdown spectroscopy (LIBS), part II: Review of instrumental and methodological approaches to material analysis and applications to different fields. *Appl. Spectrosc.* **2012**, *66*, 347–419. [CrossRef]
14. Ren, J.; Zhao, Y.; Yu, K. LIBS in agriculture: A review focusing on revealing nutritional and toxic elements in soil, water, and crops. *Comput. Electron. Agric.* **2022**, *197*, 106986. [CrossRef]
15. Rodriguez-Pascual, J.A.; Doña-Fernández, A.; Loarce-Tejada, Y.; De Andres-Gimeno, I.; Valtuille-Fernández, E.; Gutiérrez-Redomero, E.; Gomez-Laina, F.J. Assessment of gunshot residue detection on a large variety of surfaces by portable LIBS system for crime scene application. *Forensic Sci. Int.* **2023**, *353*, 111886. [CrossRef]
16. Dib, S.R.; Nespeca, M.G.; Santos Junior, D.; Ribeiro, C.A.; Crespi, M.S.; Gomes Neto, J.A.; Ferreira, E.C. CN diatomic emission for N determination by LIBS. *Microchem. J.* **2020**, *157*, 105107. [CrossRef]
17. Lu, C.; Wang, B.; Jiang, X.; Zhang, J.; Niu, K.; Yuan, Y. Detection of K in soil using time-resolved laser-induced breakdown spectroscopy based on convolutional neural networks. *Plasma Sci. Technol.* **2018**, *21*, 034014. [CrossRef]
18. Erler, A.; Riebe, D.; Beitz, T.; Löhmannsröben, H.-G.; Gebbers, R. Soil Nutrient Detection for Precision Agriculture Using Handheld Laser-Induced Breakdown Spectroscopy (LIBS) and Multivariate Regression Methods (PLSR, Lasso and GPR). *Sensors* **2020**, *20*, 418. [CrossRef]
19. Babos, D.V.; Tadini, A.M.; De Morais, C.P.; Barreto, B.B.; Carvalho, M.A.R.; Bernardi, A.C.C.; Oliveira, P.P.A.; Pezzopane, J.R.M.; Milori, D.M.B.P.; Martin-Neto, L. Prediction of exchangeable Ca and Mg in soils by laser-induced breakdown spectroscopy and chemometrics. *Catena* **2024**, *239*, 107914. [CrossRef]
20. Pelagio, M.C.; Navarro, D.A.; Janik, L.J.; Lamorena, R.B. Potential application of laser-induced breakdown spectroscopy (LIBS) data for the determination of cation exchange capacity (CEC) of agricultural soils. *ChemistrySelect* **2020**, *5*, 3798–3804. [CrossRef]
21. He, Y.; Liu, X.; Lv, Y.; Liu, F.; Peng, J.; Shen, T.; Zhao, Y.; Tang, Y.; Luo, S. Quantitative Analysis of Nutrient Elements in Soil Using Single and Double-Pulse Laser-Induced Breakdown Spectroscopy. *Sensors* **2018**, *18*, 1526. [CrossRef]
22. Ministry of Environmental Protection of the People's Republic of China. *HJ 717-2014*; Soil quality—Determination of total nitrogen—Modified Kjeldahl method. Standards Press of China: Beijing, China, 2014.
23. Ministry of Agriculture of the People's Republic of China. *NY/T 87-1988*; Fertilizer—Determination of total nitrogen content—Kjeldahl method. Standards Press of China: Beijing, China, 1988.
24. Ministry of Agriculture of the People's Republic of China. *NY/T 1121.13-2006*; Soil testing—Part 13: Method for determination of soil pH. Standards Press of China: Beijing, China, 2006.
25. Carvalho, A.A.C.; Alves, V.C.; Silvestre, D.M.; Leme, F.O.; Oliveira, P.V.; Nomura, C.S. Comparison of Fused Glass Beads and Pressed Powder Pellets for the Quantitative Measurement of Al, Fe, Si and Ti in Bauxite by Laser-Induced Breakdown Spectroscopy. *Geostand. GeoAnal. Res.* **2017**, *41*, 585–592. [CrossRef]
26. Pořízka, P.; Klus, J.; Képeš, E.; Prochazka, D.; Hahn, D.W.; Kaiser, J. On the utilization of principal component analysis in laser-induced breakdown spectroscopy data analysis, a review. *Spectrochim. Acta B At. Spectrosc.* **2018**, *148*, 65–82. [CrossRef]
27. Li, X.; He, Z.; Liu, F.; Chen, R. Fast Identification of Soybean Seed Varieties Using Laser-Induced Breakdown Spectroscopy Combined With Convolutional Neural Network. *Front. Plant Sci.* **2021**, *12*, 714557. [CrossRef]
28. Bai, X.; Zhang, C.; Xiao, Q.; He, Y.; Bao, Y. Application of near-infrared hyperspectral imaging to identify a variety of silage maize seeds and common maize seeds. *RSC Adv.* **2020**, *10*, 11707–11715. [CrossRef] [PubMed]
29. Huang, Y.; Harilal, S.S.; Bais, A.; Hussein, A.E. Progress Toward Machine Learning Methodologies for Laser-Induced Breakdown Spectroscopy With an Emphasis on Soil Analysis. *IEEE Trans. Plasma Sci.* **2023**, *51*, 1729–1749. [CrossRef]
30. Nørgaard, L.; Saudland, A.; Wagner, J.; Nielsen, J.P.; Munck, L.; Engelsen, S.B. Interval Partial Least-Squares Regression (iPLS): A Comparative Chemometric Study with an Example from Near-Infrared Spectroscopy. *Appl. Spectrosc.* **2000**, *54*, 413–419. [CrossRef]
31. Peng, J.; He, Y.; Ye, L.; Shen, T.; Liu, F.; Kong, W.; Liu, X.; Zhao, Y. Moisture Influence Reducing Method for Heavy Metals Detection in Plant Materials Using Laser-Induced Breakdown Spectroscopy: A Case Study for Chromium Content Detection in Rice Leaves. *Anal. Chem.* **2017**, *89*, 7593–7600. [CrossRef]
32. Vapnik, V.; Chapelle, O. Bounds on Error Expectation for Support Vector Machines. *Neural Comput.* **2000**, *12*, 2013–2036. [CrossRef]
33. Feng, L.; Zhu, S.; Chen, S.; Bao, Y.; He, Y. Combining Fourier Transform Mid-Infrared Spectroscopy with Chemometric Methods to Detect Adulterations in Milk Powder. *Sensors* **2019**, *19*, 2934. [CrossRef]
34. Viscarra Rossel, R.A.; McGlynn, R.N.; McBratney, A.B. Determining the composition of mineral-organic mixes using UV–vis–NIR diffuse reflectance spectroscopy. *Geoderma* **2006**, *137*, 70–82. [CrossRef]
35. Lu, Y.; Du, C.; Yu, C.; Zhou, J. Fast and nondestructive determination of protein content in rapeseeds (Brassica napusL.) using Fourier transform infrared photoacoustic spectroscopy (FTIR-PAS): Determination of protein content in rapeseeds using FTIR-PAS. *J. Sci. Food Agric.* **2014**, *94*, 2239–2245. [CrossRef]
36. Jia, L.; Liu, X.; Xu, W.; Xu, X.; Li, L.; Cui, Z.; Liu, Z.; Shu, R. Initial Drift Correction and Spectral Calibration of MarSCoDe Laser-Induced Breakdown Spectroscopy on the Zhurong Rover. *Remote Sens.* **2022**, *14*, 5964. [CrossRef]

37. Xu, X.; Ma, F.; Zhou, J.; Du, C. Applying convolutional neural networks (CNN) for end-to-end soil analysis based on laser-induced breakdown spectroscopy (LIBS) with less spectral preprocessing. *Comput. Electron. Agr.* **2022**, *199*, 107171. [CrossRef]
38. Irvine, S.; Andrews, H.; Myhre, K.; Goldstein, K.; Coble, J. Radiative transition probabilities of neutral and singly ionized Europium estimated by laser-induced breakdown spectroscopy (LIBS). *J. Quant. Spectrosc. Radiat. Transf.* **2022**, *286*, 108184. [CrossRef]
39. Shaaban, K.; Hamdi, A.; Ghanim, M.; Shaban, K.B. Machine learning-based multi-target regression to effectively predict turning movements at signalized intersections. *Int. J. Transp. Sci. Technol.* **2023**, *12*, 245–257. [CrossRef]
40. Kordos, M.; Arnaiz-González, Á.; García-Osorio, C. Evolutionary prototype selection for multi-output regression. *Neurocomputing* **2019**, *358*, 309–320. [CrossRef]
41. Wang, N.; Er, M.J.; Han, M. Parsimonious Extreme Learning Machine Using Recursive Orthogonal Least Squares. *IEEE Trans. Neural Netw. Learn. Syst.* **2014**, *25*, 1828–1841. [CrossRef] [PubMed]
42. Zhang, D.; Zhang, H.; Zhao, Y.; Chen, Y.; Ke, C.; Xu, T.; He, Y. A brief review of new data analysis methods of laser-induced breakdown spectroscopy: Machine learning. *Appl. Spectrosc. Rev.* **2020**, *57*, 89–111. [CrossRef]
43. Do, N.-T.; Hoang, V.-P.; Doan, V.S. A novel non-profiled side channel attack based on multi-output regression neural network. *J. Cryptogr. Eng.* **2023**, *14*, 427–439. [CrossRef]
44. Xue, B.; Chang, B.; Du, D. Multi-Output Monitoring of High-Speed Laser Welding State Based on Deep Learning. *Sensors* **2021**, *21*, 1626. [CrossRef] [PubMed]
45. Kamilaris, A.; Prenafeta-Boldú, F.X. Deep learning in agriculture: A survey. Comput. *Electron. Agric.* **2018**, *147*, 70–90. [CrossRef]
46. Saharia, C.; Ho, J.; Chan, W.; Salimans, T.; Fleet, D.J.; Norouzi, M. Image Super-Resolution Via Iterative Refinement. *IEEE Trans. Pattern Anal. Mach. Intell.* **2022**, *45*, 4713–4726. [CrossRef] [PubMed]

Disclaimer/Publisher's Note: The statements, opinions and data contained in all publications are solely those of the individual author(s) and contributor(s) and not of MDPI and/or the editor(s). MDPI and/or the editor(s) disclaim responsibility for any injury to people or property resulting from any ideas, methods, instructions or products referred to in the content.